Two-photon Absorption Properties of BODIPYs-like compounds based on BF_2-naphthyridine Complexes

Journal:	*Physical Chemistry Chemical Physics*
Manuscript ID	CP-ART-10-2018-006580.R1
Article Type:	Paper
Date Submitted by the Author:	26-Feb-2019
Complete List of Authors:	Dipold, Jessica; Universidade de São Paulo, FCM Romero, Eduardo; University of Central Florida, Department of Chemistry Donnelly, Julie; University of Central Florida, Chemistry Calheiro, Tainara; Universidade Federal de Santa Maria, Departamento de Química Bonacorso, Helio; Universidade Federal de Santa Maria, Departamento de Química; Federal University of Santa Maria Iglesias, Bernardo; Universidade Federal de Santa Maria, Chemistry; Siqueira, Jonathas; Instituto de Física de São Carlos, Universidade de São Paulo, Departamento de Física e Ciência dos Materiais Boni, Leonardo; IFSC - USP, FCM Hernandez, Florencio; University of Central Florida, the College of Optics and Photonics, Mendonça, Cleber Renato; Universidade de São Paulo, FCM

Two-photon Absorption Properties of BODIPYs-like compounds based on BF_2-naphthyridine Complexes

Jessica Dipold[1], Eduardo E. Romero[2], Julie Donnelly[2], Tainara P. Calheiro[3], Helio G. Bonacorso[3*], Bernardo A. Iglesias[4*] , Jonathas P. Siqueira[1], Florencio E. Hernandez[2,5], Leonardo De Boni[1], Cleber R. Mendonca[1*]

[1]Instituto de Física de São Carlos, Universidade de São Paulo, Caixa Postal 369, 13560-970 São Carlos, SP, Brazil.

[2]Department of Chemistry, University of Central Florida, P. O. Box 162366, Orlando, USA.

[3]Núcleo de Química de Heterociclos (NUQUIMHE), Departamento de Química, Universidade Federal de Santa Maria, Santa Maria, RS, 97105-900, Brazil.

[4]Departamento de Química, Laboratório de Bioinorgânica e Materiais Porfirínicos, Universidade Federal de Santa Maria, 97105-900, Santa Maria, RS, Brazil.

[5]CREOL/The College of Optics and Photonics, University of Central Florida, P. O. Box 162366, Orlando, USA.

**Correspondence to: crmendon@ifsc.usp.br, +551633738077; helio.bonacorso@ufsm.br, +55 3220 8756; bernardopgq@gmail.com, +55 55 32208671.*

Keywords: Naphthyridines; Two-photon absorption; Density Function Theory.

Abstract

Boron dipyrromethenes type molecules (BODIPYs) are versatile molecules which have been used for applications ranging from photodynamic therapy to solar cells (DSSC). However, these molecules usually do not present high two-photon absorption cross-sections, limiting their use in nonlinear optical applications. Herein, we study a series of BF_2-napthyridine based boron-complexes with electron-donating and withdrawing groups to increase their two-photon absorption. We have found two-photon absorption cross-sections up to approximately 270 GM, which corresponds to an increase of approximately five times in comparison to the average cross-section value reported for molecules with similar conjugation length,

pointing out such compounds as potential material for nonlinear applications in both visible and infrared spectral regions.

1. Introduction

In last years, Borondipyrromethene (BODIPY) derivatives have been drawing considerable interest because of their potential applications[1], which includes, but are not limited to, light-harvesting systems[2], agents in photodynamic therapy[3], biomolecular labels[4, 5], laser dyes[6] and sensitizer for solar cells[7]. This large variety of applications are related to the BODIPYs-like inherent features, such as photochemical and chemical stability, easy solubility, high fluorescence yields and molar absorption coefficients, long excited-state lifetimes and sharp fluorescence peaks ranging from the blue to the infrared region[8].

Molecular systems containing the 1,8-naphthryridine derivatives have also been used as "*organic scaffolds*" to construct BF_2 compounds in the last years due to their good fluorescence properties and biocompatibility[9]. These molecules possess a heterocyclic moiety which is an attractive tool for identification of novel biological potential[10]. The BF_2-type organoboron compounds based on 1,8-naphthyridine heterocycles are used as fluorescent dyes due to their high fluorescence quantum yields[11, 12] and high photochemical stabilities[5, 13]. Their good fluorescence properties[14] and large Stokes shifts[15, 16] have been extensively reported in the literature.

Two-photon absorption (2PA) processes hold interest for several applications, such as micromachining[17], optical power limiting[18], photodynamic therapy[19] and two-photon absorption fluorescence spectroscopy[20]. Disposed to increase the range and effectiveness of such applications, several studies have involved the synthesis of novel compounds in order to enhance the 2PA cross-sections of molecules, each one focused on a particular use[21].

In general, BODIPYs structures do not present good 2PA cross-sections, having an average value in the range of 50 GM[21-24] in visible wavelengths. Since these molecules still have other promising characteristics, especially its high

fluorescence quantum yield, methods have been developed to improve their 2PA capabilities. In this direction, for instance, increasing the conjugation length[21] has brought the two-photon absorption cross-section of this class of molecules up to 150 GM, while changing the conjugation length and adding electron-donating and electron-withdrawing groups to the BODIPYs types main structure[25, 26] have led 2PA cross-sections to values of the order of 400 GM. Such approaches, however, results in larger molecules with complex structures, composed of several electron withdrawing and electron donating groups.

In this paper, we determined the two-photon absorption spectra of seven BF2-naphthyridine molecules[15] with either one or two electron donating or electron withdrawing groups attached, therefore keeping a simpler molecular structure. Two-photon absorption cross-section values as high as 270 GM were observed, which corresponds to an increase of about five times in comparison to the average experimentally measured cross-section value reported for molecules with similar conjugation length. Such results point to the use of this class of materials as potential candidates for the development of applications from photodynamic therapy agents[3] to biomolecular labels [4, 5], for instance.

2. Experimental Section

2.1 Studied organoboron complexes

In this work, we have studied a series of seven novel 9-aryl-3-(aryl/heteroaryl)-1,1-difluoro-7-(trifluoromethyl)-1H[1,3,5,2]oxadiazaborinino[3,4-a][1,8]naphthyridin-11-ium-1-uide complexes. Structural representation of the BF_2-complexes are displayed in Fig. 1 with the corresponding labels. Their synthetic methodology and structural/spectroscopic characterization, as well as fluorescence emission and electrochemical properties, have been already reported elsewhere[15].

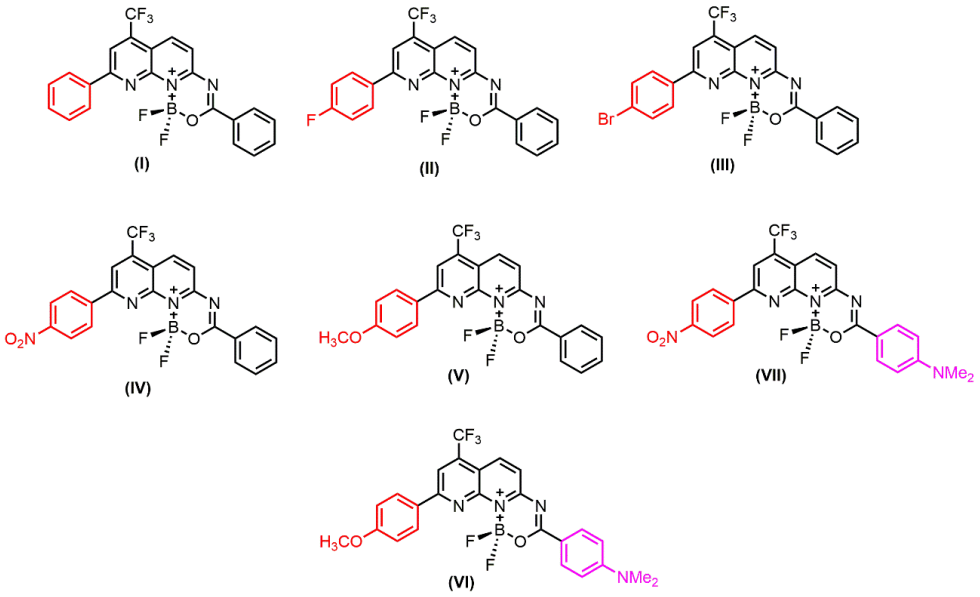

Fig. 1: Representative structures of the seven studied BF2-complexes.

2.2 Two-photon absorption measurements

Samples were diluted in dichloromethane (DCM) in concentrations ranging from 10^{-2} to 10^{-3} M for the nonlinear absorption measurements and 10^{-4} M for linear ones. Linear and two-photon absorption measurements were performed in 2 mm optical path quartz cells. The linear absorption spectra were obtained by a UV-1800 Shimatzu spectrometer.

The 2PA spectra were obtained through the open-aperture Z-Scan technique[27]. A Ti:Sapphire laser amplifier (775 nm - CPA-2001 system from Clark-MXR Inc.), delivering pulses with a duration of 150 fs at a 1 kHz repetition rate, is used as the excitation source for an Optical Parametric Amplifier (OPA) that delivers 120 fs pulses in the wavelength range of 470 – 1200 nm. Spatial filtering is performed before the Z-scan setup in order to ensure a Gaussian beam profile. In the Z-scan technique, the sample is translated through the focal plane of a Gaussian beam (z-direction), while its transmittance is measured in the far field. For a sample with nonlinear absorption, its absorbance depends on the beam intensity according to $\alpha = \alpha_0 + \beta I$, in which α_0 is its linear absorption coefficient, β is the 2PA coefficient, and *I* is the intensity of the beam. The transmitted power for

a Gaussian beam can be integrated over time, for each wavelength, giving the normalized transmittance as

$$T(z) = \frac{1}{\sqrt{\pi} q_0(z,0)} \int_{-\infty}^{\infty} ln\left[1 + q_0(z,0) e^{-\tau^2}\right] d\tau \quad (1),$$

in which,

$$q_0 = \beta I_0 L \left(1 + \left(\frac{z^2}{z_0^2}\right)\right)^{-1}, \quad (2).$$

I_0 is the intensity of the laser beam, L is the length of the sample, z is the sample position and z_0 is the Rayleigh length. The 2PA coefficient, β, is then obtained by fitting the experimental transmittance curve using equation Eq. 1. Once β is determined, it is possible to calculate the two-photon absorption cross-section (σ_{2PA}) using

$$\sigma_{2PA} = \frac{\hbar \omega \beta}{N}, \quad (3),$$

in which ω is the excitation wavelength, and N is the number of molecules/cm^3. The 2PA cross-section is usually expressed in Göppert-Mayer (GM) units, in which 1 GM = 10^{50} cm^{4}s/photon.

3. Theoretical approach

All quantum chemistry calculations were performed using density functional theory (DFT)[28]. The molecular structure of all complexes was optimized through the Becke's three parameter exchange, Lee, Yang and Parr correlation (B3LYP) hybrid functional[29-31] and the standard Pople's 6-31G(d,p) basis set[32] employing the Gaussian 09 package[33]. Solvent effects (dichloromethane) were considered through the optimization process using the polarizable continuum model (PCM) [34, 35]. All the optimized structures were verified to be a real minimum through frequency analysis.

The 2PA transition probabilities calculations were carried out using time dependent density functional theory (TD-DFT) in DALTON 13[36]. Solvent effects were considered using the polarizable continuum model (PCM)[34, 35]. Atom-centered cavities were used with the same radius as given by the G09 package. The cavity radii are 1.4430 Å, 2.0415 Å, 1.9255 Å, 1.8300 Å, 1.750 Å, 1.6820 Å, and 2.0950 Å for H, B, C, N, O, F, and Br atoms respectively with alpha = 1.100. The Hybrid

B3LYP functional[29-31] was employed in combination with the Pople's 6-311G(d) [32] basis set. The 20 lowest-energy states were calculated for each molecule.

The 2PA cross sections were obtained using the 2PA transition probabilities as follows:

$$\delta_{0f}^{TPA}(\omega) = \frac{4\pi\alpha {a_0}^5}{c}\sum_f (\hbar\omega_f)^2 \overline{\delta}_{0f}^{TPA}(\omega_{0f}) g(2\omega,\omega_{0f},\mathbf{\Gamma}), \quad (4),$$

$$\overline{\delta}_{0f}^{TPA}(\omega_{0f}) = \frac{1}{30}\left(2\sum_{a,b} S_{aa}{S_{bb}}^* + 4\sum_{a,b} S_{ab}{S_{bb}}^*\right), \quad (5),$$

$$g(2\omega,\omega_{0f},\mathbf{\Gamma}) = \frac{1}{\pi}\frac{\Gamma_{gf}/2}{(\omega_{gf}-2\omega)^2 + (\Gamma_{gf}/2)^2} \quad (6),$$

Equation 4 represents the 2PA cross section. In Eq. 4, c is the speed of the light in vacuum, α is the fine structure constant, E=$\hbar\,\omega$ is the photon energy (in the degenerate case half of the transition energy), a_0 is the Bohr radius, and $\overline{\delta}_{0f}^{TPA}(\omega_{0f})$ is the orientation averaged two-photon transition probability for the degenerate case defined by Eq. 5. A Lorentzian line-shape $g(2\omega,\omega_{0f},\mathbf{\Gamma})$ was used in order to broaden the electronic transitions (Eq. 6.), where Γ is the full width at half maximum (FWHM). The obtained TPA cross-sections are represented in Göpper-Mayer units (GM), i.e., 10^{-50} $cm^4.s.mol^{-1}.photon^{-1}$, when atomic units are used for $\overline{\delta}_{0f}^{TPA}(\omega_{0f})$, ω, and Γ_{gf} and cgs units are used for a_0 and c [37].

The actual excited states used for the analysis were obtained after removing weak oscillator strength states, as well as states that were out of the experimental range. Since the experimental measurements were done using a ~10 nm bandwidth laser beam, we convoluted states in this range into a single excited state. With this approach, we used the oscillator strength and predicted wavelength to build Lorentzian curves around each band, giving rise to the predicted spectrum, in which the FWHM of every absorption line was set to 0.2 eV.

4. Results and Discussion

All molecules were dissolved in DCM with concentrations of 10^{-4} M for the linear absorption measurements. For compound **I**, which presents the basic structure of all molecules studied in this work (phenyl units), the linear absorption spectrum is shown as a dashed line in Fig. 2. As it can be seen, compound **I** presents a peak around 270 nm and two narrow bands around 400 nm. The band around 270 nm can be related to the intraligand $\pi \rightarrow \pi^*$ transition, while the ones around 400 nm come from the $n \rightarrow \pi^*$ transition ($S_0 \rightarrow S_1$)[15]. The peaks around 400 nm show vibrational progression, which is associated with transitions between non-localized conjugated states (S_1), with a spacing of ~170 meV, which is in agreement with the C=C and C=N vibrational modes of the naphthyridine in the complex[16]. TD-DFT calculations at the theoretical level B3LYP/6-31G(d,p) for 20 electronic transitions are in agreement with the experimental results as shown in Fig. 2a for compound **I**. The low energy band corresponds to a HOMO → LUMO (98%) transition centered at 399 nm with negligible charge transfer exhibiting a $n \rightarrow \pi^*$ transition (Fig. 4a), while the second transition is centered at 275 nm corresponding to the molecular orbitals HOMO-1→ LUMO+1(77%), HOMO → LUMO+2(10%), and HOMO-6 → LUMO(5%) presenting a predominant intraligand $\pi \rightarrow \pi^*$ electronic transition.

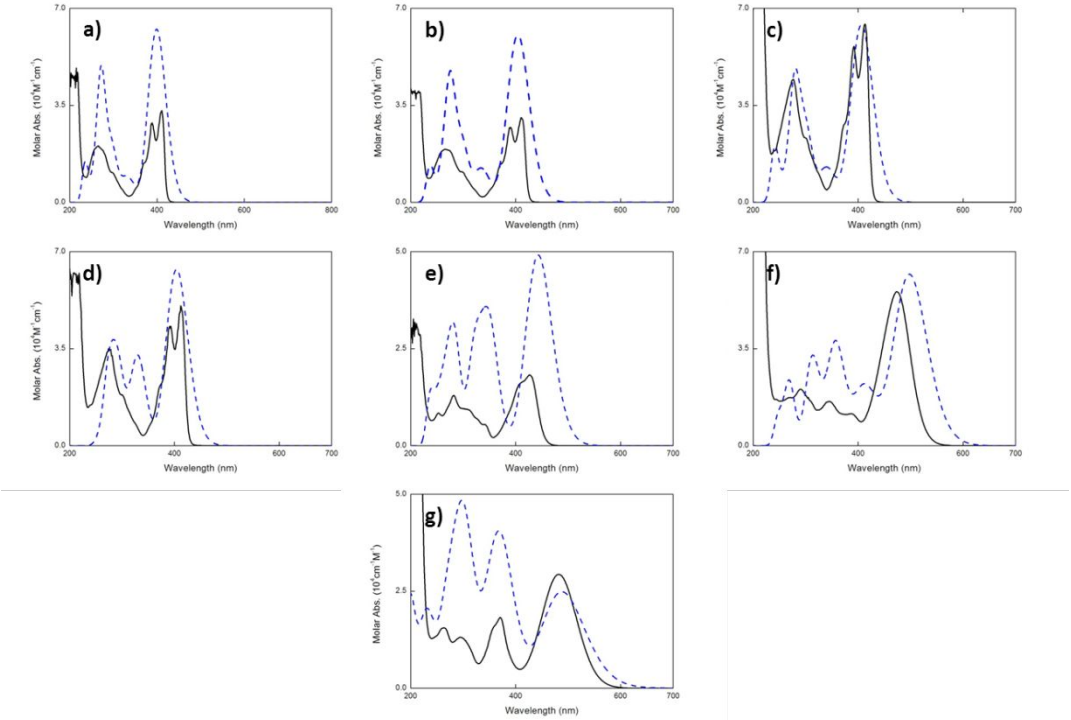

Fig. 2: Experimental UV-Visible spectra (solid black line) and theoretical UV-Visible (dashed blue line) for compounds (a) **I**, (b) **II**, (c) **III**, (d) **IV**, (e) **V**, (f) **VI**, (g) **VII**.

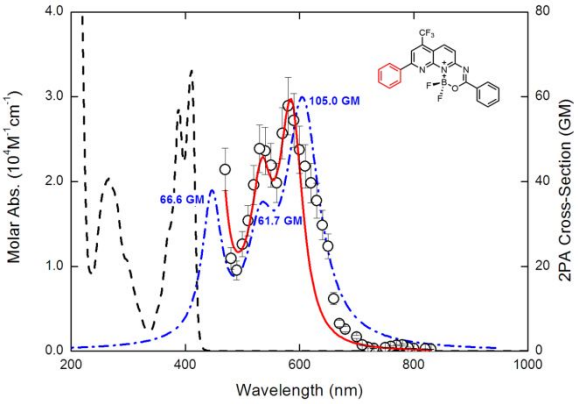

Fig. 3: Experimental 2PA spectra (circles) with sum-over-states (SOS) fitting (red line) and calculated states (dot-dashed blue line), as well as the molar absorptivity (one-photon absorption) (dashed black line) for compound **I**. The values close to each peak in the theoretical 2PA spectrum indicate the magnitude of the 2PA cross-section.

For the nonlinear measurements, solutions were prepared using DCM with concentrations from 10^{-2} to 10^{-3} M. Open-aperture Z-scan measurements were carried out to obtain the two-photon absorption cross-section spectrum, which was

fitted by using a sum-over-states (SOS) model and compared to the theoretically calculated 2PA states.

In the SOS, the 2PA is described by a dipolar contribution, related to the two-photon transition to the first excited state, followed by contributions from higher electronic states, which are determined from both the linear and 2PA measurements. The resonant enhancement contribution to the nonlinear effect is also considered in this model, and it is related to the first excited state. For the molecules studied in this paper, we used energy diagrams with four or five energy levels, considering the ground state (0). For a general energy level diagram, the SOS expression is given by[38-42]

$$\sigma_{ng}^{(2)}(\omega) = \frac{4(2\pi)^5}{5(hc)^2} L^4 \omega^2 \left\{ \frac{|\vec{\mu}_{01}|^2 |\overrightarrow{\Delta\mu}_{01}|^2}{\omega^2} g_{01}(2\omega) + \sum_n \frac{|\vec{\mu}_{01}|^2 |\vec{\mu}_{1n}|^2}{(\omega_{0n} - \omega)^2 + \Gamma_{0n}^2(\omega)} g_{0n}(2\omega) \right\} \quad (7),$$

in which, c is the light speed, h is the Planck's constant, and ω is the excitation laser frequency. L is the Onsager field factor, $L = \frac{3n_{ref}^2}{2n_{ref}^2} + 1$, with n_{ref} = 1.41 (refractive index for DCM[43]), used to take into account effects of the medium in the complexes. ω_{0n}, Γ_{0n} and μ_{mn} are the angular frequency of the light, the damping constant and the transition dipole moment of n→m electronic transitions, respectively. $\Delta\mu_{01}$ is the difference between the permanent dipole moments of the ground state and the first excited state, and $g_{0n}(\omega)$ is the lineshape of the two-photon absorption to a final state m, given by a Lorentzian. ω_{0n} and Γ_{0n} are obtained from fitting the peaks seen in the linear absorption spectrum, while μ_{mn} and $\Delta\mu_{01}$ are fitting parameters. In Eq. 7, the dipolar term is the one related to $g_{01}(2\omega)$, while the non-dipolar ones are within the summation. The parameter μ_{01} was obtained experimentally from the linear absorption spectrum, considering the angular frequency and the molar absorptivity of the first excited state[44, 45].

For the studied compounds, three different energy diagrams were considered depending on the compound $\Delta\mu_{01}$ value. If the first 2PA transition was related to the first band of the linear absorption spectrum, the dipolar term was considered in the SOS fitting and $\Delta\mu_{01} \neq 0$. Otherwise, the dipolar term was not

taken into account since $\Delta\mu_{01}$ can be neglected and an extra term was added to the sum, adding an energy-level to the energy-level diagram.

The open circles in Fig. 3 correspond to the 2PA cross-section spectrum for compound **I**, in which two peaks can be observed, as well as the resonant enhancement region starting at about 500 nm. The first peak is at 530 nm, with a 2PA cross-section of 47 GM, while the second one is located at 580 nm with a 2PA cross-section of 58 GM, which is of the same order as previously measured BODIPY-like molecules with this short conjugation length. In order to describe the 2PA spectrum of this molecule, we employed a four-energy-level diagram for the SOS model, not considering the dipolar term since the first 2PA band is not related to the first linear absorption band. In Table 1, the first line shows the parameters obtained from the fitting (red line in Fig. 3) for compound **I**.

The 2PA spectrum is directly related to the compound high energy band in the linear absorption. Therefore, we can assume they come from the intraligand $\pi \rightarrow \pi^*$ transition band. The dot-dashed (blue) line in Fig. 3 corresponds to the 2PA spectrum determined through TD-DFT quadratic response calculations; the values close to each peak indicate the magnitude of the 2PA cross-section theoretically calculated. As it can be seen, there is a good agreement between the shape and spectral position of the 2PA bands. However, the theoretical cross-sections are overestimated by the B3LYP functional, which may be attributed to the lack of long-range interaction within the functional. CAMB3LYP, which includes long and short-range interactions, is not able to represent correctly the shape and transition energies of the studied compound, indicating that the discrepancy not only comes from the inclusion of long-range interactions, but from the amount of correlation and exchange in the functional. In Fig. 4a, the low energy electronic transition (HOMO→LUMO) is shown for compound **I**. The HOMO-LUMO transition exhibits a small charge transfer character between the extremity rings towards the center, which is almost negligible, explaining the low observed 2PA cross-sections for it.

Table 1: Fitted parameters of the SOS model for all compounds.

Compound	μ_{01} (D)	$\Delta\mu_{01}$ (D)	λ_{01} (nm)	Γ_{01} (10^{14} Hz)	μ_{12} (D)	λ_{02} (nm)	Γ_{02} (10^{14} Hz)	μ_{13} (D)	λ_{03} (nm)	Γ_{03} (10^{14} Hz)	μ_{14} (D)	λ_{04} (nm)	Γ_{04} (10^{14} Hz)
I	5.9	-	394	0.9	6.0	294	0.9	3.3	268	0.9	2.5	227	1.0
II	5.7	-	395	0.9	5.2	294	0.8	3.4	267	0.8	2.2	234	1.0
III	5.7	-	397	0.9	5.0	318	0.8	5.0	280	0.9	3.6	231	1.0
IV	6.9	-	393	0.9	7.2	294	0.6	4.0	268	0.8	3.8	231	0.8
V	7.9	4.8	426	0.8	7.3	337	0.8	3.1	270	0.9	2.3	240	0.8
VI	8.6	8.7	482	0.7	7.8	385	0.9	6.5	300	0.8	-	-	-
VII	10.5	13.0	492	0.8	6.1	368	0.8	3.8	303	0.8	-	-	-

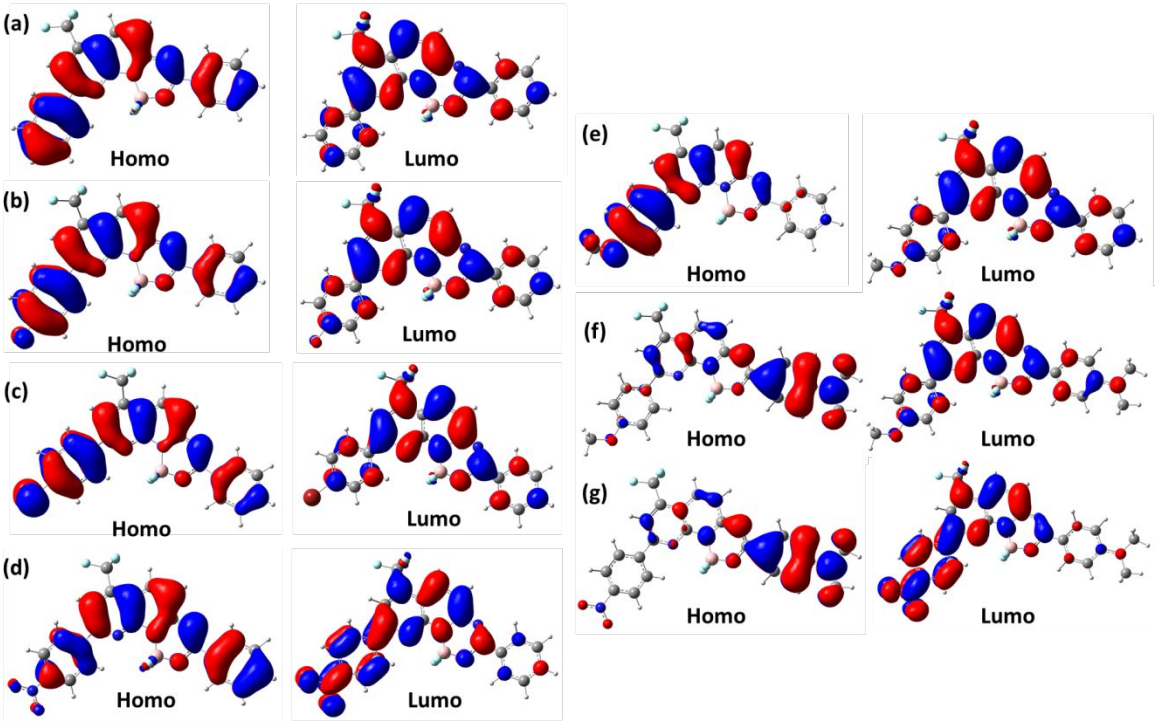

Fig. 4: Orbital HOMO→LUMO transitions for compounds (a) **I**, (b) **II**, (c) **III**, (d) **IV**, (e) **V**, (f) **VI** and (g) **VII** calculated for the highest 2PA transitions through TD-DFT.

The linear absorption spectra for compounds **II**, **III** and **IV**, shown respectively in Fig. 5a-c, present features similar to the one of compound **I** (Fig. 3 – dashed line); such molecules are composed of the same core as compound **I** with a different group bonded into the para position of one of its phenyl rings. Those groups are intrinsic acceptor groups, however F and Br atoms are able to donate electron density by resonance, which explains the difference in intensity of the $n\rightarrow$

π^* and $\pi \rightarrow \pi^*$ transition bands observed in Fig. 5a-c. The overlapping of carbon and fluorine p-orbitals is more effective than in bromine as consequence of fluorine being located in the second row of the periodic table, effect that is in agreement with the difference in spectral signatures between compounds **II** and **III** and explains the spectral similarity of compound **III** with compound **IV**. On the other hand, compound **V** linear absorption spectrum does not present the vibrational progression on its 400 nm band, as shown in Fig. 5d; such molecule presents an electron donating group bonded into the para position in one of its phenyl rings. The donating electron group reduces the gap between the C=C and C=N vibrational modes and modifies the $\pi \rightarrow \pi^*$ transition band in respect to compounds **II**, **III** and **IV**. Fig. 2b-d shows the experimental and theoretical (20 states at B3LYP/6-31-G(d,p)) UV-Visible spectrum of compounds **II**, **III**, **IV** and **V**. The calculated theoretical spectra are in agreement with the first two experimental low-energy electronic transition bands. Compounds **II**, **III**, **IV** and **V** low-energy theoretical transitions correspond to a HOMO→LUMO transition centered at 404 nm (98%), 406 nm (98%), 404 nm (97%) and 443 nm (99 %). The HOMO→LUMO transition orbitals in compounds **II**, **III**, and **IV** exhibit negligible charge transfer behavior where the electron density localized in the phenyl rings is reduced upon excitation into the LUMO orbital of compounds **II** and **III** (donors by resonance), while in compound **IV** the density increases towards the para nitrobenzene ring, which can be explained by the resonance electron withdrawing character of the nitro group, but non-large charge separation is observed (see Fig. 4b-d). Compound **V** exhibits a similar behavior in its low-energy electronic transition (HOMO→LUMO), however, Fig. 4e shows a slight difference in the electron density distribution on the HOMO orbital. The density is localized toward the Anisole ring while the non-functionalized phenyl ring presents a negligible electron density distribution, exhibiting an opposed behavior in respect to compound **IV,** where the density is partially localized on the nitrobenzene ring. The HOMO→LUMO transition in compound **V** presents a small charge transfer behavior as consequence of the methoxy donating group that induces electron delocalization through resonance. The latter have a stronger resonance donor behavior in

comparison with Fluorine and Bromine (compounds **II** and **III**), causing charge separation during the HOMO→ LUMO electronic transition. Additionally, the small charge transfer behavior explains why the theoretical low-energy transition presents a small red shift compared with the experimental spectrum shown in Fig. 2e (~16 nm).

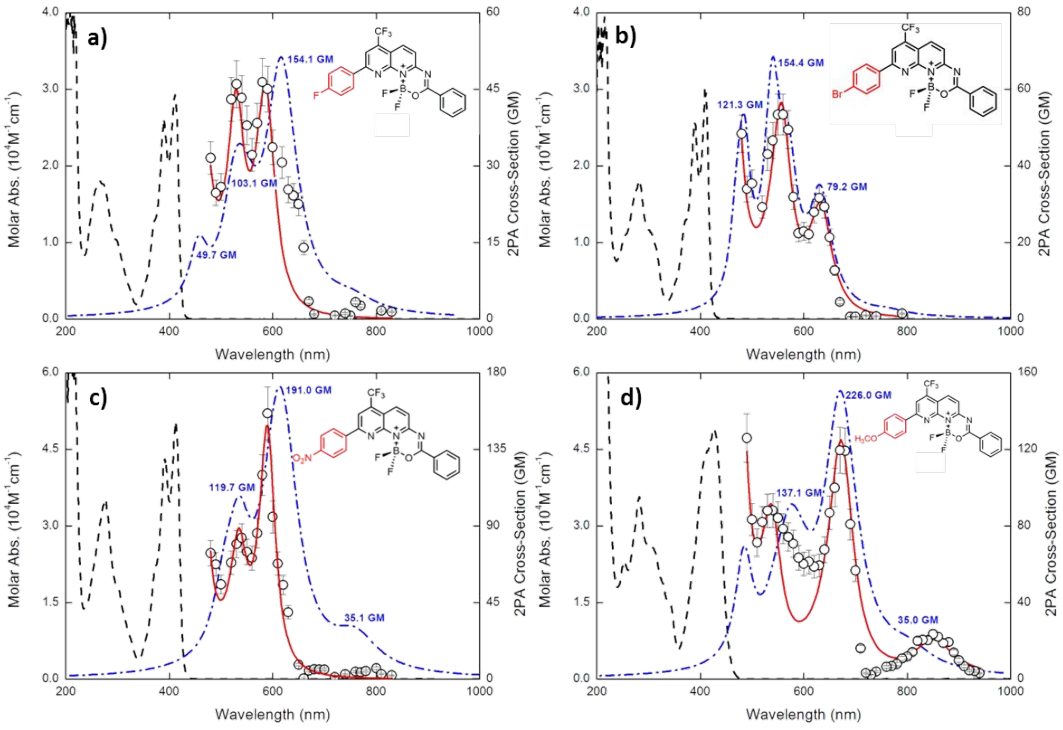

Fig. 5: Linear absorption spectra (dashed lines) for BF_2-complex derivatives II (a), III (b), IV (c) and V (d). The circles correspond to the 2PA spectra with its SOS fitting (red line). The blue dot-dashed line represents the position and amplitude of the calculated 2PA. The values close to each peak in the theoretical 2PA spectrum indicate the magnitude of the 2PA cross-section.

The open circles in Fig. 5 show the 2PA cross-section spectra for compounds **II**, **III**, **IV**, and **V**. Since the linear absorptions are similar for molecules **II**, **III**, and **IV**, it was expected that their 2PA spectra also present similar shapes, as seen in Fig. 5. Also, such 2PA results are similar to the ones observed for compound **I** (Fig. 3). Compound **II** (Fig. 5a) presents two 2PA peaks with about the same magnitude, one at 530 nm and the other one at 580 nm, both with 46 GM. Its theoretical 2PA spectrum (dashed blue line) overestimates the cross-sections, but

its peak position is in agreement with the experimental data with a small deviation in shape that may be attributed to the lack of exchange and correlation in the functional. The bromine derivative (compound **III**) exhibits a larger 2PA cross-section, with a value of approximately 53 GM at 560 nm, and a smaller one of 32 GM at 630 nm. The opposite behavior is observed in compound **IV** (nitro group), which presents a smaller 2PA cross-section peak (~83 GM) at 540 nm and a larger one (~156 GM) at 590 nm. The 2PA theoretical spectra of compounds **III** and **IV** are in agreement with the experimental findings mentioned previously. The 2PA cross-sections are overestimated by the functional in compound **III**, however the functional is able to estimate appropriately the cross-section of **IV**. In both compounds the theoretical approach is able to reproduce adequately the experimental shape and peaks positions, in contrast with compound **II** where the shape is not completely accurate but works for comparison purposes. For compound **V**, containing a donor group (CH_3O) bonded to the phenyl ring, a 2PA peak at around 850 nm (~24 GM) is observed, which corresponds to the electronic state at 400 nm observed in the linear absorption spectrum. This feature is probably related to the dipolar characteristic of this molecule. The same behavior was also observed for compounds **VI** and **VII,** as will be shown later. It has a larger peak of 120 GM at 670 nm, and a smaller one at 540 nm with 88 GM. Compounds **IV** and **V** have a 2PA cross-section of the same order as previously measured BODIPY molecules[24]. Compound **V** theoretical 2PA spectrum (Fig. 5d blue-dashed line) presents a peak position and shape equivalent to its experimental counterpart, reproducing the low and high-energy two-photon electronic transitions. However, the cross-sections are overestimated by a factor 2 in respect to the largest intensity peak, which indicates that the B3LYP functional is not able to reproduce accurately the cross-sections, but it is capable to reproduce the spectral positions as well as the relative intensities.

Since compounds **II**, **III**, and **IV** (Fig 5. a-c) display two 2PA peaks that are not related to their first linear absorption band, as well as a resonant enhancement peak, a four-energy-level diagram without the dipolar term was used in the SOS approach to model the data. For compound **V** (Fig. 5d), a five-energy-level diagram,

considering the dipolar term, was employed. All the parameters obtained from the SOS fitting are also summarized in Table 1.

In this context, BF_2-naphthyridine derivative **I** presents a similar maximum 2PA cross-section to compound **II**, followed by compounds **III** and **IV**. From Fig. 4, the charge transfer that happens in the HOMO→LUMO transition for compounds **II** (Fig. 4b) and **III** (Fig. 4c) are similarly negligible, both happening from the rings towards the center of the compound. Compound **IV** (Fig. 4d), however, presents a small charge transfer into the withdrawing electron group (nitro) from the right to the left side of the molecule, which explains the largest 2PA cross-section observed in it. Compound **V** (Fig. 4e) presents a comparable maximum 2PA cross-section due to its push-pull like transition as compound **IV**, which happens between the two extremities of the molecule. Since the electron density is pulled more efficiently by the nitro group in compound **IV** than given by the methoxy in compound **V,** we observe a larger 2PA cross-section in compound **IV**. Also, the pull-push like behavior of compounds **VI** and **V** is the responsible in the increase of the cross-sections relative to compound **I**.

The linear absorption spectra for compounds **VI** and **VII** are shown as dashed lines in Fig. 6 a-b. Both present small peaks from 260 to 390 nm, and a stronger peak around 480 nm. Such molecules also present a red shift in their linear absorption spectrum in comparison to the other ones, possibly due to an intra-molecular charge transfer band, related to its strong push-pull structure [16]. Figure 2f-g shows the experimental and theoretical (20 states B3LYP/6-31G(d,p)) UV-Vis spectrum of compounds **VI** and **VII**. The level of theory employed is able to reproduce with an acceptable accuracy the spectral shape and position of the first two low-energy electronic transitions. In both molecules the lowest energy electronic transition corresponds to a pure HOMO→LUMO transition (**VI** 98%, **VII** 99%). The theoretical UV-Vis of compound **VI** (Fig. 2f) exhibits a small red shift of ~25 nm that is comparable with the one observed in compound **V,** which contains the same methoxy donor group. The larger red shift can be justified by the additional dimethylamine donor group located in the second phenyl ring in the para position which is able to donate electron density into the π–system, making

B3LYP not completely suitable for an exact description of compound **VI**. This compound does not present a typical push-pull structure with an electron donor and an electron attractor at the extremes of the molecule, however, its first electronic transition exhibits a large charge transfer as can be seen in Fig. 4f, were the HOMO presents a localized density towards the N,n-Dimethylaniline ring, while the LUMO exhibits a larger density distribution into the Anisole ring comparable with the one observed in the LUMO of compound **V** (Fig. 4e). The push-pull character of **VI** can be explained in terms of p-orbital overlap as well as electronegativity. Nitrogen presents an atomic radius and a p-orbital size comparable with carbon, allowing a better carbon-heteroatom overlapping in comparison with oxygen, which makes Nitrogen a better donor by resonance. Additionally, Oxygen presents a larger electronegativity than Nitrogen, making it a better acceptor group. The overall effect on the molecule, at least in its lower energy electronic transition, is making it a pseudo push-pull system where the donating electron group is Dimethylamine at the N,n-Dimethylaniline ring, while the attracting electron group is located at the Anisole ring (methoxy group). On the other hand, compound **VII** presents a pure push-pull behavior, where the donating electron group is located at the N,n-Dimethylaniline ring (dimethylamine group) while the accepting electron group is located at the nitrobenzene ring (nitro group). Fig. 4g shows that the lowest energy electronic transition presents a strong charge transfer behavior, with the HOMO orbital presenting a large localized density towards the N,n-Dimethylaniline ring (similar to compound **VI**) while the LUMO presents a localized density along the nitrobenzene ring (similar to compound **IV**) showing a well-defined charge separation during its excitation. The theoretical UV-Vis spectrum of compound **VII** (Fig. 2g) is in agreement with the experimental one, exhibiting a similar shape and spectral position, indicating that B3LYP is able to model and reproduce the properties of compound **VII** without the inclusion of long-range interactions as it was mentioned for the previous analyzed molecules.

The 2PA spectra for molecules **VI** and **VII** are shown in Fig. 6a-b (open circles). They present similar shapes, with two main 2PA peaks; for compound **VI** the peaks are located at 770 and 960 nm, with magnitudes of 148 and 80 GM,

while in the nonlinear spectrum for compound **VII** the peaks are at 730 and 990 nm, with magnitudes of 210 and 268 GM. Such a result corresponds to an increase of approximately five fold, as compared to the average cross-section value reported for molecules with similar conjugation length, and are of the same order of recently studied BODIPY compounds[26] with larger conjugation length and several electron-donating or electron-withdrawing groups.

In Table 1, we show the fitted parameters for these two molecules with the SOS model, presented in Fig. 6a-b as a continuous red line. For these molecules a four-level energy diagram was used for the fitting, considering the dipolar term.

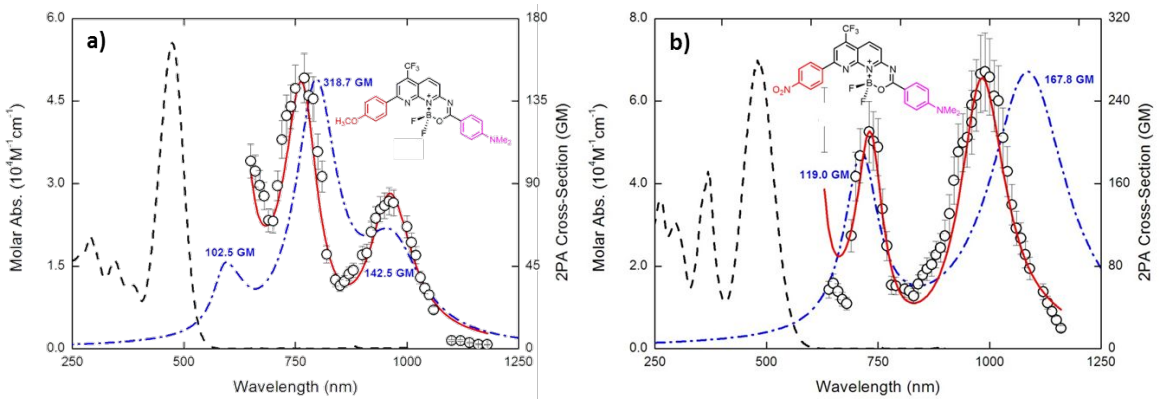

Fig. 6: Two-photon absorption spectra (circles) with SOS fitting (red line) and calculated states (blue dot-dashed line), as well as the linear absorption (dashed black line) for compounds a) **VI** and b) **VII**. The values close to each peak in the theoretical 2PA spectrum indicate the magnitude of the 2PA cross-section.

For both molecules the lowest energy 2PA peak observed in the spectrum matches the band at about 480 nm of the linear absorption spectrum. Such absorption is attributed to a $n \rightarrow \pi$ transition and, therefore, has a more meaningful contribution for compound **VII**, which contains NO_2 and NMe_2 groups. The high energy peak is red-shifted for compound **VII**, which is related to its strong ICT, once strong donor (NMe_2) and acceptor (NO_2) groups are bonded to the *para*-position of phenylene aromatic rings (like push-pull systems) of this compound. The theoretical 2PA spectrum of compounds **VI** and **VII** is shown in Fig. 6a-b (blue dashed line). The theoretical 2PA spectrum of compound **VI** is in agreement with the experimental one, with equivalent peak positions and relative intensities, however, the cross-sections are overestimated as in the previous studied molecules. On the other hand, compound **VII** theoretical 2PA spectrum exhibits a

red shift in respect to its low-energy electronic transition of ~97 nm, and the 2PA cross-sections are underestimated by B3LYP, though the peaks relative intensities are comparable with the experimental results. This result can be explained by the large intermolecular charge transfer that the compound presents, due to the presence of a strong acceptor (Nitro) and donor group (dimethylamine) which makes theB3LYP functional not completely suitable for the description of the 2PA spectrum of **VII**. Long-range interactions were included to calculate the 2PA spectrum of **VII** (CAM-B3LYP), but the shape and peaks positions were not as accurate as those obtained with the B3LYP functional, indicating that the amount of exchange and correlation in the functional may place an important part in the description of the studied molecules.

From compound **VI** and **VII** HOMO-LUMO transition, presented on Fig. 4f and 4g, it is possible to see a difference between the moving charges pattern for both compounds. On compound **VI** there is an evident charge transfer from the dimethyl amine into the first half of the molecule during the transition, while for compound **VII** there is a large charge transfer from the NMe_2 group to the NO_2 group, creating a push-pull structure since the two ligands are located in opposite sides of the molecule. Since the charge transfer is much larger for compound **VII**, it presents a larger 2PA cross-section value than compound **VI**.

We also compared the 2PA states found through quadratic response calculations with the maxima observed in the 2PA spectra. This comparison is summarized in Table 2. The wavelength of the calculated spectra for the compounds was shifted from 50 to 60 nm towards the blue, which is within the usual deviation of the theory. For compounds **I** to **VI**, the calculated wavelengths and the measured ones had differences of 35 nm at most, while compound **VII** had a larger disagreement with ~97 nm. This bigger difference in the wavelength value, as well as of the calculated 2PA cross-section, happens due to the zwitterionic character and the charge transfer characteristics of the studied compound. Examining the obtained data, we can conclude that the inclusion of donating or accepting groups into the molecule increases its 2PA cross-sections considerably, and this increment depends on the capacity of such groups to withdraw or donate

electron density towards the π system of the molecule. Compounds **II** and **III** do not exhibit a large difference in cross-sections in respect to compound **I** as consequence that their acceptor efficiency is determined mostly by induction effects. Compounds **IV** and **V** present a single strong acceptor and donor electron group respectively that pull or push electron density through the π system by resonance, which explains the increment in cross-sections in both compounds. The difference in 2PA cross-sections between compounds **IV** and **V** can be related to a better p orbital overlapping between carbon and nitrogen than between carbon and oxygen, as well as a large charge delocalization toward the oxygen atoms in the nitro group. On the other hand, compounds **VI** and **VII** present two molecular groups bonded into the main BODIPY-like core. Compound **VI** presents two electron donating groups by resonance and attractors by induction (methoxy and dimethylamine groups), both competitive effects that makes the max 2PA cross-section smaller than in the case of compound **IV**, but stronger than compound **V** due to the additional donating group. The combination of both donating an acceptor groups increases considerably the 2PA cross-sections due to a large charge separation during their electronic transition as consequence of an excellent charge delocalization through the π-system, and can be observed in compound **VII**, which presents a strong resonance attracting group (nitro group) as well as a strong resonance donating group (dimethylamine group), exhibiting a 2PA cross-section of almost two times larger than compounds **IV** and **VI**. Our theoretical results exhibit a different trend in respect to the experimental cross-sections, however, the peak position and relative intensities are in agreement with the experimental results as it was mentioned previously. Despite of B3LYP functional not being able to reproduce appropriately the 2PA cross-sections magnitude of these molecules due to their zwitterionic and charge transfer nature, which makes the 2PA transition probabilities being either over or underestimated, it is still a powerful functional for the prediction of the peak positions as well as the correct spectral shape.

Table 2: Comparison between the maximum 2PA cross-section calculated through DFT with the measured ones for compounds **II**, **III**, **IV**, **V, VI, VII**.

Compound	λ_{2PA} theo. (nm)	σ_{2PA} theo. (GM)	λ_{2PA} exp. (nm)	σ_{2PA} exp. (GM)
II	529	91	530	46
III	560	73	550	53
IV	612	197	590	156
V	670	227	670	120
VI	796	319	770	148
VII	1065	168	990	268

To verify our measured data further, the dipole moments for each compound were also calculated through DFT, and their values are compared to the ones measured experimentally in Table 3.

Table 3: Dipole moments measured and calculated for all compounds.

Compound	Measured μ_{01} (D)	Theoretical μ_{01} (D)	Measured μ_{12} (D)	Theoretical μ_{12} (D)	Measured μ_{13} (D)	Theoretical μ_{13} (D)	Measured μ_{14} (D)	Theoretical μ_{14} (D)
I	5.9	6.7	6.0	4.0	3.3	1.9	2.5	1.7
II	5.7		5.2		3.4		2.2	
III	5.7	4.0	5.0	4.0	5.0	2.3	3.6	1.0
IV	6.9	8.6	7.2	10.15	4.0	1.9	3.8	2.4
V	7.9	6.8	7.3	12.2	3.1	3.6	2.3	2.3
VI	8.6	17	7.8	12.6	6.5	2.0	-	-
VII	10.5	30.9	6.1	5.9	3.8	1.3	-	-

Compounds **I** to **V** present good agreement between theoretically and experimentally obtained dipole moments, all of them being of the same order of magnitude and with differences smaller than 5 D. However, for compounds **VI** and **VII** the differences are much larger, particularly for the first dipole moment (μ_{01}). This was caused by the previously mentioned issues with the large amount of charge transfer present in these compounds, which led to an overestimation of their two-photon absorption cross-sections as well as their dipole moments.

5. Conclusion

We studied the two-photon absorption cross-section spectra of a series of seven new BF_2-naphthyridine molecules, developed to have a larger 2PA cross-section than previous ones. The compounds with largest 2PA cross-section were

compound **VII**, with a 2PA cross-section of 268 GM at 990 nm, and compound **IV**, with a 2PA cross-section of 156 GM at 590 nm, while the molecule with the smallest 2PA cross-section was compound **II**, with 46 GM at 580 nm. Considering previous studies of BODIPYs compounds, most of them present intricate structures to increase their conjugation length and internal charge transfer to obtain 2PA cross-sections of up to 350 GM in the visible region. In the present paper the studied molecules revealed cross-sections of the same order with a simpler structure, demonstrating that these compounds have a good potential for nonlinear applications in both visible and near infrared spectral regions.

Conflicts of Interest

There are no conflicts to declare.

Acknowledgments

This study was financed in part by the Coordenação de Aperfeiçoamento de Pessoal de Nível Superior - Brasil (CAPES) - Finance Code 001, FAPESP #2016/20886-1, CNPq, Army Research Laboratory W911NF-17-1-0123, Air Force Office of Scientific Research (FA9550-12-1-0028) and Research Support Foundation of the State of Rio Grande do Sul (FAPERGS) (PqG, process number 17/2551-0001275-5). We thank STOKES ARCC for the computational time provided for the completion of this research

References

1. R. Ziessel, G. Ulrich and A. Harriman, *New Journal of Chemistry*, 2007, **31**, 496-501.
2. X. L. Zhang, Y. Xiao and X. H. Qian, *Organic Letters*, 2008, **10**, 29-32.
3. J. F. Lovell, T. W. B. Liu, J. Chen and G. Zheng, *Chemical Reviews*, 2010, **110**, 2839-2857.
4. Y. Urano, D. Asanuma, Y. Hama, Y. Koyama, T. Barrett, M. Kamiya, T. Nagano, T. Watanabe, A. Hasegawa, P. L. Choyke and H. Kobayashi, *Nature Medicine*, 2009, **15**, 104-109.
5. S. H. Alamudi, R. Satapathy, J. Kim, D. D. Su, H. Y. Ren, R. Das, L. N. Hu, E. Alvarado-Martinez, J. Y. Lee, C. Hoppmann, E. Pena-Cabrera, H. H. Ha, H. S. Park, L. Wang and Y. T. Chang, *Nature Communications*, 2016, **7**.
6. C. F. A. Gomez-Duran, I. Garcia-Moreno, A. Costela, V. Martin, R. Sastre, J. Banuelos, F. L. Arbeloa, I. L. Arbeloa and E. Pena-Cabrera, *Chemical Communications*, 2010, **46**, 5103-5105.

7. S. Hattori, K. Ohkubo, Y. Urano, H. Sunahara, T. Nagano, Y. Wada, N. V. Tkachenko, H. Lemmetyinen and S. Fukuzumi, *Journal of Physical Chemistry B*, 2005, **109**, 15368-15375.
8. A. C. Benniston and G. Copley, *Physical Chemistry Chemical Physics*, 2009, **11**, 4124-4131.
9. J. L. Katz, B. J. Geller and P. D. Foster, *Chemical Communications*, 2007, 1026-1028.
10. L. Fu, X. Feng, J. J. Wang, Z. Xun, J. D. Hu, J. J. Zhang, Y. W. Zhao, Z. B. Huang and D. Q. Shi, *Acs Combinatorial Science*, 2015, **17**, 24-31.
11. J. Zheng, F. Huang, Y. J. Li, T. W. Xu, H. Xu, J. H. Jia, Q. Ye and J. R. Gao, *Dyes and Pigments*, 2015, **113**, 502-509.
12. H. G. Bonacorso, T. P. Calheiro, B. A. Iglesias, C. H. da Silveira, E. N. da Silva, A. Ketzer, F. Bublitz, N. Zanatta and M. A. P. Martins, *Journal of Fluorine Chemistry*, 2018, **205**, 8-14.
13. H. G. Bonacorso, T. P. Calheiro, B. A. Iglesias, T. V. Acunha, S. Z. Franceschini, A. Ketzer, A. R. Meyer, L. V. Rodrigues, P. A. Nogara, J. B. T. Rocha, N. Zanatta and M. A. P. Martins, *New Journal of Chemistry*, 2018, **42**, 1913-1920.
14. S. Hikishima, N. Minakawa, K. Kuramoto, Y. Fujisawa, M. Ogawa and A. Matsuda, *Angewandte Chemie-International Edition*, 2005, **44**, 596-598.
15. H. G. Bonacorso, T. P. Calheiro, B. A. Iglesias, I. R. C. Berni, E. N. da Silva, J. B. T. Rocha, N. Zanatta and M. A. P. Martins, *Tetrahedron Letters*, 2016, **57**, 5017-5021.
16. Y. Y. Wu, Y. Chen, G. Z. Gou, W. H. Mu, X. J. Lv, M. L. Du and W. F. Fu, *Organic Letters*, 2012, **14**, 5226-5229.
17. D. S. Correa, M. R. Cardoso, V. Tribuzi, L. Misoguti and C. R. Mendonca, *Ieee Journal of Selected Topics in Quantum Electronics*, 2012, **18**, 176-186.
18. T. C. Lin, G. S. He, Q. D. Zheng and P. N. Prasad, *Journal of Materials Chemistry*, 2006, **16**, 2490-2498.
19. Z. Huang, *Technology in Cancer Research & Treatment*, 2005, **4**, 283-293.
20. W. Denk, J. H. Strickler and W. W. Webb, *Science*, 1990, **248**, 73-76.
21. L. W. Barros, J. A. Castaneda, T. A. S. Cardoso, D. K. Kolmel, A. Horner, A. Bihlmeier, M. Nieger, S. Brase, C. H. D. Cruz, L. A. Padilha and Ieee, San Jose, CA, 2016.
22. Y. C. Wang, D. K. Zhang, H. Zhou, J. L. Ding, Q. A. Chen, Y. Xiao and S. X. Qian, *Journal of Applied Physics*, 2010, **108**.
23. L. Porres, O. Mongin and M. Blanchard-Desce, *Tetrahedron Letters*, 2006, **47**, 1913-1917.
24. Q. D. Zheng, G. X. Xu and P. N. Prasad, *Chemistry-a European Journal*, 2008, **14**, 5812-5819.
25. B. Kucukoz, G. Sevinc, E. Yildiz, A. Karatay, F. Zhong, H. Yilmaz, Y. Tutel, M. Hayvali, J. Zhao and H. G. Yaglioglu, *Physical Chemistry Chemical Physics*, 2016, **18**, 13546-13553.
26. L. W. T. Barros, T. A. S. Cardoso, A. Bihlmeier, D. Wagner, D. K. Kolmel, A. Horner, S. Brase, C. H. B. Cruz and L. A. Padilha, *Physical Chemistry Chemical Physics*, 2017, **19**, 21683-21690.
27. M. Sheikbahae, A. A. Said, T. H. Wei, D. J. Hagan and E. W. Vanstryland, *Ieee Journal of Quantum Electronics*, 1990, **26**, 760-769.
28. E. Runge and E. K. U. Gross, *Physical Review Letters*, 1984, **52**, 997-1000.
29. A. D. Becke, *Physical Review A*, 1988, **38**, 3098-3100.
30. A. D. Becke, *Journal of Chemical Physics*, 1993, **98**, 5648-5652.
31. C. T. Lee, W. T. Yang and R. G. Parr, *Physical Review B*, 1988, **37**, 785-789.
32. M. J. Frisch, J. A. Pople and J. S. Binkley, *Journal of Chemical Physics*, 1984, **80**, 3265-3269.
33. M. J. Frisch, G. W. Trucks, H. B. Schlegel, G. E. Scuseria and M. A. Robb, et. al., *Journal*, 2013.
34. J. Tomasi, B. Mennucci and E. Cances, *Journal of Molecular Structure-Theochem*, 1999, **464**, 211-226.
35. J. Tomasi, B. Mennucci and R. Cammi, *Chemical Reviews*, 2005, **105**, 2999-3093.

36. K. Aidas, C. Angeli, K. L. Bak, V. Bakken, R. Bast, L. Boman, O. Christiansen, R. Cimiraglia, S. Coriani, P. Dahle, E. K. Dalskov, U. Ekstrom, T. Enevoldsen, J. J. Eriksen, P. Ettenhuber, B. Fernandez, L. Ferrighi, H. Fliegl, L. Frediani, K. Hald, A. Halkier, C. Hattig, H. Heiberg, T. Helgaker, A. C. Hennum, H. Hettema, E. Hjertenaes, S. Host, I.-M. Hoyvik, M. F. Iozzi, B. Jansik, H. J. A. Jensen, D. Jonsson, P. Jorgensen, J. Kauczor, S. Kirpekar, T. Kjrgaard, W. Klopper, S. Knecht, R. Kobayashi, H. Koch, J. Kongsted, A. Krapp, K. Kristensen, A. Ligabue, O. B. Lutnaes, J. I. Melo, K. V. Mikkelsen, R. H. Myhre, C. Neiss, C. B. Nielsen, P. Norman, J. Olsen, J. M. H. Olsen, A. Osted, M. J. Packer, F. Pawlowski, T. B. Pedersen, P. F. Provasi, S. Reine, Z. Rinkevicius, T. A. Ruden, K. Ruud, V. V. Rybkin, P. Salek, C. C. M. Samson, A. S. de Meras, T. Saue, S. P. A. Sauer, B. Schimmelpfennig, K. Sneskov, A. H. Steindal, K. O. Sylvester-Hvid, P. R. Taylor, A. M. Teale, E. I. Tellgren, D. P. Tew, A. J. Thorvaldsen, L. Thogersen, O. Vahtras, M. A. Watson, D. J. D. Wilson, M. Ziolkowski and H. Agren, *Wiley Interdisciplinary Reviews-Computational Molecular Science*, 2014, **4**, 269-284.
37. Y.-Z. Lan, *Chemical Physics Letters*, 2012, **545**, 95-99.
38. P. A. Franken and J. F. Ward, *Reviews of Modern Physics*, 1963, **35**, 23-&.
39. B. J. Orr and J. F. Ward, *Molecular Physics*, 1971, **20**, 513-&.
40. C. W. Dirk, L. T. Cheng and M. G. Kuzyk, *International Journal of Quantum Chemistry*, 1992, **43**, 27-36.
41. R. R. Birge and B. M. Pierce, *Journal of Chemical Physics*, 1979, **70**, 165-178.
42. K. Kamada, K. Ohta, I. Yoichiro and K. Kondo, *Chemical Physics Letters*, 2003, **372**, 386-393.
43. J. E. Bertie, Z. Lan, R. N. Jones and Y. Apelblat, *Applied Spectroscopy*, 1995, **49**, 840-851.
44. M. G. Vivas, D. L. Silva, L. De Boni, Y. Bretonniere, C. Andraud, F. Laibe-Darbour, J. C. Mulatier, R. Zalesny, W. Bartkowiak, S. Canuto and C. R. Mendonca, *Journal of Physical Chemistry B*, 2012, **116**, 14677-14688.
45. J. Dipold, R. Batista, R. D. Fonseca, D. L. Silva, G. L. C. Moura, J. V. dos Anjos, A. M. Simas, L. De Boni and C. R. Mendonca, *Chemical Physics Letters*, 2016, **661**, 143-150.

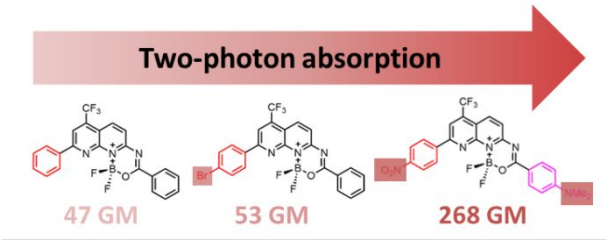

High two-photon absorption cross-sections of BODIPY-like compounds were obtained for simple structures.